Surface Reconstruction for Computer Vision-based Craniofacial Surgery

S.M. Bhandarkar[1], A.S. Chowdhury[1], E.W. Tollner[2], J.C. Yu[3], E.W. Ritter[3], A. Konar[4]
[1]Dept. of Computer Science
[2]Dept. of Biol. & Agr. Engr.
The University of Georgia
Athens, GA 30602, USA.
[3]Dept. of Plastic Surgery
Medical College of Georgia
Augusta, GA 30912, USA
[4]Dept. of Electronics & Telecommunication Engr.
Jadavpur University
Kolkata, India

Abstract

High-energy traumatic impact of the craniofacial skeleton is an inevitable consequence of today's fast paced society. The work presented in the paper addresses the problem of craniofacial reconstruction using two popular surface matching algorithms namely the Iterative Closest Point (ICP) algorithm and the Data Aligned Rigidity Constrained Exhaustive Search (DARCES) algorithm. The two algorithms are first applied individually and then in combination to achieve the desired reconstruction. The synergistic combination of the DARCES and ICP algorithms is found to yield higher reconstruction accuracy in much shorter execution time compared to the ICP algorithm used in isolation. The local surface irregularities on the fracture surfaces are exploited using a fuzzy set theoretic approach and a curvature-based method. Incorporation of the knowledge of the surface irregularities by means of two reward-penalty schemes in the hybrid DARCES-ICP algorithm is shown to result in robust and accurate surface reconstruction. Experimental results on Computer Tomography (CT) image data obtained from fractured human mandibles are presented.

Keywords: DARCES, ICP, Mean and Gaussian Curvatures, Fuzzy sets, Computer Tomography (CT).

1. Introduction

High-energy traumatic impact of the craniofacial skeleton is an inevitable consequence of today's fast paced society. The plastic surgeon restores the form and function of the fractured bone elements in the craniofacial skeleton, typically, by first exposing all the bone fragments, then returning them to their normal configuration, and finally maintaining the aligned bone fragments with rigid screws and plates. However, there are several critical and inherent limitations to this current, standard approach. To visualize the fragments, in order to align them, necessitates their exposure which consequently reduces the attached blood supply. To improve the blood supply, one can decrease the extent of dissection. However this means not being able to visualize the entire fracture, which could lead to potential mal-alignments of the bone fragments. We seek to solve the above dilemma by developing an enabling technology that leverages recent advances in computer vision, computer visualization and computer-aided design/manufacturing (CAD/CAM) to reconstruct the craniofacial skeleton and align the fracture surfaces *in silico.* The reconstruction of the craniofacial skeleton from broken fragments is achieved by using the Iterative Closest Point (ICP) [1] and the Data Aligned Rigidity Constrained Exhaustive Search (DARCES) [4] algorithms. Bipartite graph matching is used to determine the corresponding surface point pairs in the ICP algorithm [2, 3]. A synergistic combination of the two algorithms, where the output of the DARCES algorithm is fed as input to the ICP algorithm, is shown to result in an improved surface matching algorithm with a substantial reduction in both, the mean squared error (MSE) as well as the execution time for the reconstruction of the craniofacial skeleton when compared to the ICP algorithm used in isolation. Further improvement in the reconstruction accuracy is achieved by labeling the pixels on the opposing fracture surfaces and incorporating the label information into the surface matching algorithms using two reward-penalty schemes proposed in this paper; one based on a fuzzy set-theoretic approach and the other based on local surface curvature characterization using the mean and Gaussian surface curvature values. The remainder of the paper is organized as follows: Section 2 describes the basic image preprocessing tasks, Section 3 describes the DARCES, ICP and hybrid DARCES-ICP algorithms, Sections 4 and 5 discuss the surface irregularity extraction procedures, Section 6 describes the two reward-penalty schemes, Section 7 presents the experimental results, and finally Section 8

Proceedings of the Seventh IEEE Workshop on Applications of Computer Vision (WACV/MOTION'05)
0-7695-2271-8/05 $ 20.00 IEEE

concludes the paper with an outline for future research.

2. Image Preprocessing

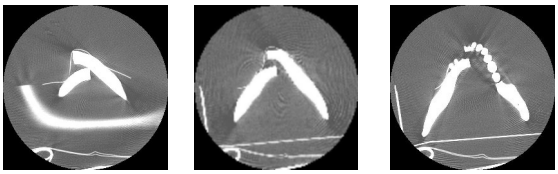

Figure 1. A typical sequence of 2D CT image slices

The input to the system (Fig.1) is a sequence of 2D grayscale images of a fractured human mandible, generated via Computer Tomography (CT). Each image slice is 150 mm x 150 mm with an 8-bit color depth. A series of image preprocessing tasks are undertaken before using the surface matching algorithms to obtain the desired goal of craniofacial reconstruction. The software resulting from the implementation of the surface matching algorithms and image preprocessing tasks is currently integrated into a JAVA-based package called *InSilicoSurgeon* [11] (© The University of Georgia Research Foundation Inc., 2004) for computer-assisted reconstructive plastic surgery. A brief description of the image preprocessing tasks is as follows:

2.1. Thresholding

In the given set of CT images, the bright areas represent the broken mandible fragments and the dark areas, the soft tissue. A simple thresholding scheme is used to binarize each CT image slice. Using a priori knowledge, we classify a pixel with gray-scale value above 250 to belong to a broken mandible fragment and represent it using the color black (Fig. 2b). The resulting binary image $B(i, j)$ for a gray scale CT image slice $G(i, j)$ given by:

$$B(i,j) = \begin{cases} 0 & \text{if} \quad G(i,j) > 250 \\ 1 & \text{otherwise} \end{cases} \qquad (1)$$

2.2. Connected Component Labeling

Binarization by itself cannot help distinguish between the two fracture fragments (Fig. 2b) since we still need to filter out some undesired artifacts so that only the broken fragments are used for the purpose of surface matching. A 2D Connected Component Labeling (CCL) algorithm in conjunction with an area filter is used to remove these unwanted artifacts (which are typically small in size). Connected components with area less than a threshold value (1000 in our case) are deleted. The result of these operations is illustrated in Fig. 2c. The results of the 2D CCL algorithm are propagated across the CT image slices, resulting in a 3D CCL algorithm.

2.3. Interactive Contour Detection

The task of interactive contour detection is performed on the results of the thresholding, CCL and size filtering operations on all the 2D CT slices. The interactive contour detection algorithm requires the user to click on the end points of each fracture contour in each of the CT slices. The intervening contour points are automatically generated using a contour tracing algorithm. The contour points from the CT image stack are assembled to form a 3D surface point data set. A 3D surface point data set is thus generated for each fracture surface. The data sets resulting from two opposable fracture surfaces are referred to as the sample data set and the model data set.

(a) (b) (c)

Figure 2. (a) Typical 2D CT slice, (b) Result of binary thresholding on (a) and (c) Result of CCL and size filtering on (b).

3. Surface Matching Algorithms

For matching two opposable fracture surfaces, first the ICP and DARCES algorithms are applied individually. Next, a synergistic combination of the two algorithms, termed as the hybrid DARCES-ICP algorithm, is investigated.

3.1. Surface Matching Using the ICP Algorithm

The main steps in the ICP algorithm [1] are:

(a) The matching points in the model data set corresponding to points in the sample data set are determined and termed as the *closest set.* The matching point pairs are determined using the Maximum Cardinality Minimum Weight (MCMW) Bipartite Graph Matching algorithm [2] based on the Hungarian method proposed by Kuhn [3]. The 3D sample and model data sets correspond to the two disjoint vertex sets (V_1, V_2) in a bipartite graph $G(V, E)$. The edge-weight $(W_{ij} \in E)$ between any two nodes i and j (such that $i \in V_1$ and $j \in V_2$) is deemed to be the Euclidean distance between them. Note that the Euclidean distance is invariant to a 3D rigid body transformation. Thus, the edge weights are given by:

$$W_{ij} = \left[(x_i - x_j)^2 + (y_i - y_j)^2 + (z_i - z_j)^2 \right]^{1/2} \quad (2)$$

(b) The 3D rigid body transformation (3D translation and 3D rotation) that brings the two surfaces into registration is computed using the theory of quaternions [1].

(c) The computed transformation is applied to the original sample data set and the MSE between the transformed sample data points and the corresponding closest points is computed. The MSE(ε^2) is given by:

$$\varepsilon^2 = (1/N) \sum_{i=1}^{N} \| c_i - (Rs_i + T) \|^2 \quad (3)$$

where R denotes the rotation matrix, T, the translation vector, s_i, a point of the sample data set and c_i, the corresponding point in the closest set. Steps (a)-(c) are repeated with an updated sample set (generated by applying R and T obtained at the current iteration to the current sample set) until a prespecified error convergence criterion (0.001 in our case) is reached.

3.2. Surface Matching Using DARCES

The main steps in the DARCES [4] algorithm are:

(a) Reference points are selected from the sample data set. From the set of reference points, 3 control points are chosen.

(b) Based on certain geometric constraints, the corresponding 3 matching points on the model data set are determined. For the 3 reference points, there will be many such sets of 3 matching points in the model data set.

(c) For each set of 3 pairs of corresponding points (i.e. the 3 control points and one set of 3 matched model points), a 3D rigid body transformation is computed using Singular Value Decomposition (SVD) [5].

(e) Each transformation is then applied to all the sample data set points other than the 3 control points. If the distance between a transformed point and its nearest model point is below a certain threshold, then this reference point is considered to have been successfully aligned on the model surface. The total number of successfully aligned sample data points is computed for each transformation.

(f) The transformation which has successfully aligned the maximum number of data points is deemed to be the solution to the surface matching problem.

3.3. DARCES -ICP Hybrid Algorithm

. The synergistic combination of the DARCES and ICP algorithms, where the inputs to the ICP algorithm are the original model set and the sample set transformed by the DARCES algorithm, results in an improved surface matching algorithm with higher reconstruction accuracy and reduced execution time when compared to the ICP algorithm used in isolation. The ICP algorithm yields an accurate 3D rigid body transformation but is sensitive to outliers in the input data. The DARCES algorithm, on the other hand, helps in outlier rejection but the computed transformation is only approximate. In the DARCES-ICP hybrid algorithm, the pairs of matched points generated by the DARCES algorithm reduce the cardinalities of the two data sets to be matched (using bipartite graph matching) in the ICP algorithm. Consequently, the dense bipartite graph used to determine the closest set in the ICP algorithm is reduced to a sparse bipartite graph with fewer nodes and edges. The subsequent MCMW bipartite graph matching procedure in the ICP algorithm has a much lower computational complexity since it is run on a sparse bipartite graph. Also, a much lower MSE is achieved for the matching of the two fracture surfaces, since the DARCES algorithm provides a better starting point to the ICP algorithm by virtue of outlier removal.

4. Curvature-based Surface Irregularity Estimation

Surface labeling of voxels/pixels in volumetric images for feature classification is a well-known technique [6]. Our goal, in this paper, is to classify and label the individual discrete sampled points on the two fracture surfaces into various primitive surface categories based on the signs of the local mean *(H)* and the Gaussian *(K)* curvatures. The digital surface, within a local window, is approximated by an analytic surface using a least-squares surface fitting technique [7, 8]. Discrete bi-orthogonal Chebyshev polynomials [9] are used as the basis functions in a local N x N window (where $N = 5$ in our case) around each point to compute the local H and K values. The surface function estimate that minimizes the sum of squared surface fitting error within the window is given by:

$$\hat{f}(u,v) = \sum_{i,j=0}^{3} a_{i,j} \varphi_i(u) \varphi_j(v) \quad (4)$$

where the f_i*'s* are the basis functions for the Chebyshev polynomials. The coefficients of the functional approximation are given by:

$$a_{i,j} = \sum_{(u,v)=(-M,-M)}^{(u,v)=(M,M)} f(u,v) b_i(u) b_j(v) \quad (5)$$

where M*= (N-1)/2* and the b_i*'s* are the normalized versions of the polynomials f_i*'s* [7-9]. From the estimated coefficients, the first and second order partial derivatives of the fitted surface are computed. The elements of the first and second surface fundamental form matrices **G** and **B** respectively and are determined from these partial derivatives. The

mean (H) and the Gaussian (K) curvature values are estimated from the elements of the matrices **G** and **B** [8]. The signs of H and K are used to classify the surface point into one of 8 qualitative surface types (Table 1). The above procedure is repeated for each point on each of the fracture surfaces for which a valid local window exists.

Table 1. Classification of surface pixels on the basis of signs of H and K [6, 7]

	$H<0$	$H=0$	$H>0$
$K<0$	Saddle Ridge	Minimal Surface	Saddle Valley
$K=0$	Ridge Surface	Flat Surface	Valley Surface
$K>0$	Peak Surface	None	Pit Surface

5. Fuzzy Set-theoretic Approach to Surface Irregularity Extraction

Two fuzzy sets termed as *droop* and *bulge* are used to classify the fracture contour points [10]. Fuzzy set theory permits us to not only classify a contour point as a droop or bulge, but also to specify the extent of droop or bulge. The average variation of the fracture surface in a direction perpendicular to the plane of fracture is estimated and is denoted by x_{avg}. Note that a fracture surface consists of several fracture contours. For each point on each such contour, the deviation from the average i.e., $(px - x_{avg})$ is determined, where px is the x coordinate of a point p. If $px > x_{avg}$, then the point p belongs to *bulge* fuzzy set else it belongs to the *droop* fuzzy set. The goal here is to highlight the surface irregularity and subsequently be able to discriminate between the surface points on the basis of their fuzzy membership values. The fuzzy membership function used for surface labeling is given by:

$$\mu_{droop/bulge}(px) = 1 - e^{-k|px - x_{avg}|} \quad (6)$$

where $\mu_{droop/bulge}$ is the membership value of a point p (with x coordinate value px) in the fuzzy set *droop* or *bulge*, as the case may be. The constant k for a particular contour is determined by setting $\mu_{droop/bulge}$ to be very close to 1 (say 0.99) and using the maximum value of $(|x - x_{avg}|)$ for all the points on that contour. This approach for determining the value of k takes into consideration very precisely the local variations of surface coordinate value with respect to the global average of the surface coordinate value over the entire fracture surface. The above fuzzy classification procedure is performed for all points on each of the fracture surfaces.

6. Reward/Penalty Schemes

A reward/penalty scheme is introduced to emphasize the effect of the extracted surface irregularities on the process of establishing faithful correspondence. Note that every pair of corresponding points on the opposing fracture surfaces are represented by corresponding elements of the two vertex sets of a bipartite graph. With the reward/penalty scheme, edge weights (W_{ij}) between the two corresponding points i and j in equation (2) are updated by adding a penalty term $(Penalty_{ij})$ to the Euclidean Norm $(Enorm_{ij})$:

$$W_{ij} = Enorm_{ij} + \lambda Penalty_{ij} \quad (7)$$

where λ is the penalty coefficient. Two different methods are used to determine the penalty term $Penalty_{ij}$ in equation (7) consistent with the two different approaches for surface feature extraction. Accordingly, a binary reward/penalty scheme is adopted for the curvature-based surface classification method and a fuzzy reward/penalty scheme is chosen for the fuzzy set-based surface classification method.

6.1. Binary Reward/Penalty Approach

The signs of H and K for a pair of corresponding points from the two opposing fracture surfaces are examined and a reward/penalty value is assigned to the pair of corresponding points based on Table 2.

Table 2. Assignment of penalty value based on the *HK* sign values for two surface points (a negative penalty indicates reward)

Nature of the two points	Penalty
Saddle Ridge, Saddle Valley	-1.0
Ridge Surface, Valley Surface	-1.0
Flat Surface, Flat Surface	-1.0
Peak Surface, Pit Surface	-1.0
At least one of the points is unclassified	0.0
All other cases	1.0

If there exists no proper local window surrounding a point, then it is not classified into any primitive surface category based on the signs of H and K. Such a point is deemed as *unclassified.* A pair of points in which at least one of the points is unclassified, is not assigned a reward or penalty value.

6.2. Fuzzy Reward/Penalty Approach

Two separate fuzzy functions are designed to indicate reward and penalty. If the two points in a pair

of corresponding points belong to the same fuzzy set, then they receive a penalty, else they receive a reward. The need for two different functions stems from the fact that the reward is *inversely* proportional to the membership difference whereas the penalty is *directly* proportional to the membership difference.

6.2.1. Fuzzy Reward. The fuzzy reward function μ_R for two points i and j is a function of the individual membership values μ_i and μ_j of these two points in the fuzzy sets *droop* and *bulge* and is given by the following equation:

$$\mu_R(\mu_i, \mu_j) = 2/(1 + e^{(r_c * |\mu_i - \mu_j|)}) \quad (8)$$

where r_c is the reward constant. The value of r_c is chosen such that μ_R is close to 0, when $|\mu_i - \mu_j|$ is maximum (i.e., equal to 1) using the following:

$$0.01 = 2/(1 + e^{(r_c * 1)}) \quad (9)$$

6.2.2. Fuzzy Penalty. The fuzzy penalty function μ_P for two points i and j is also a function of the individual membership values μ_i and μ_j of these two points in the fuzzy sets *droop* and *bulge* and is given by:

$$\mu_P(\mu_i, \mu_j) = (1 - e^{(-p_c * |\mu_i - \mu_j|)}) \quad (10)$$

where p_c is the penalty constant. The value of p_c is chosen such that μ_P is close to 1, when $|\mu_i - \mu_j|$ is maximum (i.e., equal to 1) using the following:

$$0.99 = (1 - e^{(-p_c * 1)}) \quad (11)$$

7. Experimental Results and Analysis

The surface reconstruction algorithms were experimentally verified on CT images of simulated mandibular fractures on phantoms of the craniofacial skeleton. The reconstruction results (i.e., the MSE), obtained by using the various surface matching algorithms (described in Section 3) are shown in Table 3. The reconstructed images for the DARCES, ICP and DARCES-ICP algorithms are visually compared in Fig. 3. The reconstruction results obtained from the various reward/penalty schemes are visually indistinguishable, in spite of their yielding a lower MSE, as shown in Table 3. In Fig. 4, the projections, along each of the coordinate axes, of the 3D reconstruction obtained using the DARCES-ICP algorithm are visually compared with the corresponding projections of the original mandible (i.e., prior to fracture). Table 3 reveals that the hybrid DARCES-ICP scheme yields a lower MSE compared to the DARCES and the ICP algorithms when used in isolation. More interestingly, it is evident that proper fine tuning of the penalty coefficient term in equation (7) can further reduce the MSE. This is true for both the curvature-based as well as the fuzzy set theoretic labeling of sample points on the opposing fracture surfaces.

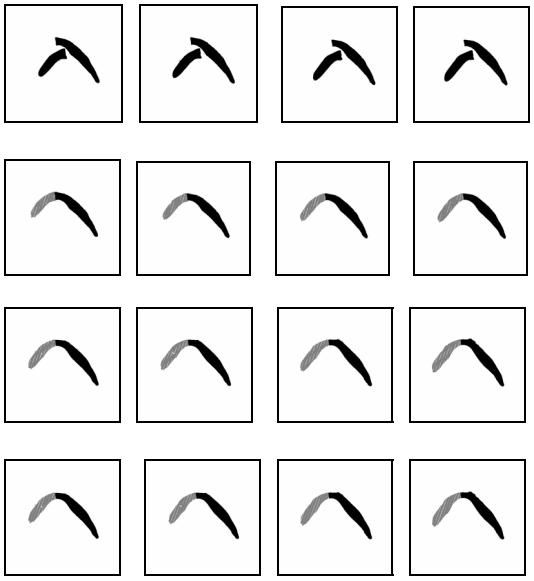

Figure 3. The first row represents a sequence of 2D slices representing the two 3D volumes (corresponding to the two fragments) to be matched. The second, third and fourth row shows the result of the ICP algorithm, the DARCES algorithm and the hybrid DARCES-ICP algorithms respectively.

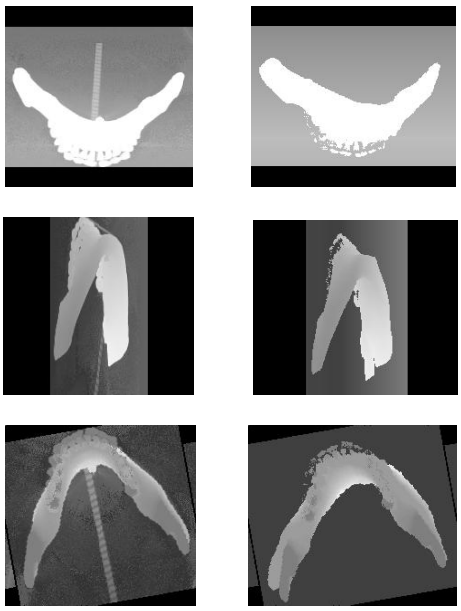

Figure 4. Comparison of the original and reconstructed mandibles. The left column is the original mandible and the right column is the reconstructed mandible obtained using the hybrid DARCES-ICP algorithm. The first, second and third rows represent the 3D projections along the x, y and z-axis respectively.

Table 3. A comparison of MSE values, obtained by applying the various surface matching algorithms

Scheme	Penalty Coeff.	MSE (mm^2)
ICP	-	0.912
DARCES	-	0.332
DARCES+ICP	-	0.251
DARCES+ICP+Fuzzy Set based Scheme	1.0	0.254
DARCES+ICP+Fuzzy Set based Scheme	0.5	0.235
DARCES+ICP+Fuzzy Set based Scheme	0.1	0.248
DARCES+ICP+Curvature based Scheme	1.0	0.252
DARCES+ICP+Curvature based Scheme	0.5	0.247
DARCES+ICP+Curvature based Scheme	0.1	0.234

8. Conclusions and Future Research

This paper addressed the problem of virtual reconstruction of the craniofacial skeleton, after having sustained mandibular fracture(s), using a set of 2D CT images as input. First, two well known surface matching algorithms, namely the ICP and DARCES were used individually to generate the virtual reconstruction. The benefits and shortcomings of the two algorithms were carefully analyzed and a synergistic combination of the two algorithms (where the output of the DARCES algorithm is fed as input to the ICP algorithm) was proposed, which resulted in a lower MSE for the virtual reconstruction. Local surface irregularities of the two opposable fracture surfaces were extracted using a local surface curvature-based approach and fuzzy set-based approach. Accordingly, two reward/penalty schemes were designed; one for the local surface curvature-based approach and the other for the fuzzy set-based approach. In the first scheme, the surface points were classified using signs of the local mean and Gaussian surface curvatures and binary penalty/reward values were assigned to the corresponding point pairs. In the second scheme, fuzzy set theory was employed for surface point classification and two fuzzy functions, one denoting a fuzzy reward and the other denoting a fuzzy penalty were used. Incorporation of the knowledge of the local surface irregularities in the bipartite graph matching procedure ensured a further improvement in the MSE with no appreciable increase in computational complexity. Future research will include judicious and/or automatic determination of the reward/penalty coefficients to yield the least possible MSE. Furthermore, the DARCES and ICP algorithms are purely data driven. In practice, in addition to obtaining a locally optimal solution, the preservation of the global 3D shape of the craniofacial skeleton is also necessary. Future enhancements will incorporate a model-driven search, guided by proper anatomical knowledge of the craniofacial skeleton, which will potentially achieve a more accurate matching of the 3D fracture surfaces as well as ensure preservation of the global 3D shape of the craniofacial skeleton. The current version of the resulting software *InSilicoSurgeon*© [11] can be used as a plug-in for the JAVA-based image processing package *ImageJ*, which is developed and distributed by the National Institutes of Health (NIH), Bethesda, Maryland, USA.

Acknowledgment: This research was supported by a Faculty of Engineering Grant from the University of Georgia Research Foundation, Athens, GA 30602, USA.

9. References

[1] P.J. Besl and N.D. McKay, A Method for Registration of 3-D Shapes, *IEEE Trans. PAMI.,* Vol. 14(2), 1992, pp. 239 – 256.

[2] W.Y. Kim and A.C. Kak, 3-D Object Recognition Using Bipartite Matching Embedded in Discrete Relaxation, *IEEE Trans. PAMI,* Vol. 13(3), 1991, pp. 224 – 251.

[3] H.W. Kuhn, The Hungarian method for the assignment problem, *Nav. Res. Log.* Quart. 2, 1955.

[4] C.S. Chen, RANSAC-Based DARCES: A New Approach to Fast Automatic Registration of Partially Overlapping Range Images, *IEEE Trans. PAMI,* Vol. 21(11), 1999, pp. 1229 – 1234.

[5] K.S. Arun, T.S. Huang and S.D. Blostein, Least-Squares Fitting of Two 3-D Point Sets, *IEEE Trans. PAMI,* Vol. 9(5), 1987, pp. 698 – 700.

[6] R. Yarger and F. Quek, Surface Parameterization in Volumetric Images for Feature Classification, *Proc. IEEE Intl. Symp. Bioinformatics and Biomed.. Engr.*, 2000, pp. 297-304.

[7] M. Suk and S.M. Bhandarkar, *Three-dimensional Object Recognition from Range Images,* Chapter 7, Springer-Verlag, Tokyo. 1992.

[8] P.J. Besl and R.C. Jain, Segmentation Through Variable-Order Surface Fitting, *IEEE Trans. PAMI.,* 10(2), 1988, pp. 167-192.

[9] R.M. Haralick, Digital Step Edges from Zero Crossing of Second Directional Derivatives*, IEEE Trans. PAMI.,* Vol. 6(1), 1984, pp. 58-68.

[10] K. Miyajima and A. Ralescu, Spatial organization in 2D segmented images: Representation and recognition of primitive spatial relations, *Fuzzy Sets and Systems,* Elsevier Science, Vol. 65, 1994, pp. 225 – 236.

[11] S.M. Bhandarkar, A.S. Chowdhury, Y. Tang, J. Yu and E.W. Tollner, Surface Matching Algorithms for Computer Aided Reconstructive Plastic Surgery, *Proc. IEEE Intl. Symp. Biomed. Imaging* (*ISBI)*, Arlington, VA, April 2004, pp. 740 – 743.